Improved embedding *ab initio* model potentials for embedded cluster calculations

José Luis Pascual,[1] Noémi Barros,[2,3] Zoila Barandiarán,[2,4] and Luis Seijo[2,4,*]

[1]*Departamento de Química Física Aplicada, C-XIV, Universidad Autónoma de Madrid, 28049 Madrid, Spain*

[2]*Departamento de Química, C-XIV, Universidad Autónoma de Madrid, 28049 Madrid, Spain*

[3]*LPCNO - Laboratoire de Physique et Chimie des Nano Objets CNRS/INSA/Uiversité de Toulouse, 135 Avenue de Rangueil, F-31077, Toulouse, France*

[4]*Instituto Universitario de Ciencia de Materiales Nicolás Cabrera, Universidad Autónoma de Madrid, 28049 Madrid, Spain*

(Dated: May 19, 2009)

Abstract

An improvement in the method of production of embedding *ab initio* model potentials (AIMP) for embedded cluster calculations in ionic solids is proposed and applied to the oxides $CeAlO_3$, CeO_2, and UO_2. The improvement affects the calculation of one of the AIMP components, the Pauli repulsion operator, which prevents the cluster electrons from collapsing onto the occupied orbitals of the host in embedded cluster calculations and, so, their over occupancy. The linear constants involved in such operator are proposed to be obtained in embedded cluster calculations in the perfect host, with the requirement that local structures calculated with working embedded clusters of relatively small size agree with those calculated with reference embedded clusters of much larger size.

I. INTRODUCTION

The embedding *ab initio* model potentials (AIMPs) for embedded cluster calculations in ionic solids have been proposed two decades ago[1] and succesfully applied in structural and spectroscopic, wave function based, quantum chemical studies of local defects created by transition metal and f-element impurities in a number of halides and oxides, both in their ground states and in large manifolds of excited states.[2,3] The most recent applications involve detailed interpretations and predictions of complex $5f$–$6d$ absorptions of actinide ions in solids under high pressure[4] and luminescence simulations of lanthanide based phosphors used in solid-state-lighting devices.[5]

The embedding AIMPs are based on the group function theory of McWeeny and Huzinaga,[6–8] which allowed for an effective differentiation in the treatment of chemically active and inactive electrons in a molecule or a solid, and supported the development of both core and embedding effective model potentials.[9–11] The embedding AIMPs are made of the following terms:[1] the electrostatic potential created by an array of point charges located at the ionic sites (Madelung potential), the electrostatic potential created by the ionic electron clouds (electron Coulomb potential), the quantum mechanical exchange operator between cluster electrons (active) and environment electrons (inactive), and the quantum mechanical Pauli repulsion operator, which prevents the cluster electrons from collapsing onto the fully occupied orbitals of the solid host, so enforcing the fulfilment of the Pauli principle. This last operator has the form $\sum_k B_k \mid \varphi_k\rangle\langle\varphi_k \mid$, where the index k runs over the occupied (frozen) orbitals of the host, φ_k, and all the B_k are positive constants that shift their orbital energies up, and so prevent their unexpected over occupancy in the self-consistent calculations on the embedded cluster.

The use of the frozen-orbital shifting operator, $\sum_k B_k \mid \varphi_k\rangle\langle\varphi_k \mid$, as a practical means to enforce the fulfilment of the Pauli principle in frozen-orbital calculations, was proposed by Huzinaga *et al.*,[7,8] who derived it in the context of frozen-core restricted variational Hartree-Fock calculations, after imposing strong-orthogonality conditions (or, more generally, linear independency conditions) between an active orbital space (the valence orbitals of a molecule) and an inactive, frozen orbital space (the core orbitals of a molecule). Huzinaga's first derivation of $B_k = -\varepsilon_k$ was later corrected by Höjer and Chung to $B_k = -2\,\varepsilon_k$.[12] This value was accepted in the frozen-core AIMP method[10,13] and model core potential (MCP)

method[14] and in the frozen-environment AIMP embedding method.[1] Although it was shown that the theory of frozen-orbital calculations justifies the use of arbitrary positive B_k values when the calculations are performed at the basis set limit,[15] Höjer and Chung's recipe seemed to work well with truncated, practical basis sets.[2] A previous recipe of $B_k = -1.5\,\varepsilon_k$ was also succesfully in use.[16]

There is, however, a problem with the definitions of the frozen-orbital shifting constants, B_k, in terms of the frozen orbital energies, ε_k, in embedded cluster calculations. The problem is related to the fact that these orbital energies include the expected value of the electrostatic potential, and the electrostatic potential of an infinite periodic solid evaluated at any point is well defined except for an arbitrary shifting constant.[17] So, although the electrostatic potential map is unique, it can be shifted down and up in energy depending on the choice of unit cell taken for its calculation, as a consequence of it being calculated with a series which is conditionally convergent, and so, it may converge on different values depending on the rearrangement of its terms.[17] As a consequence of this, two different choices of unit cells which are replicated in order to produce the embedding potential in an embedded cluster calculation, may lead to two different sets of orbital energies of the frozen embedding orbitals, ε_k, shifted respect to each other. Then, any choice of the B_k values of the type $B_k = -\lambda\,\varepsilon_k$ involves an arbitrariness, either explicit or implicit, even if λ is fixed, like the traditional choice $\lambda = 2$. Furthermore, cases are found where the choice of unit cell (and its implicitely assumed electrostatic potential reference) leads to positive orbital energies ε_k and negative B_k values; in situations like these, the frozen-orbital shifting operator does not act preventing the collapse of the active cluster orbitals onto the host but, on the contrary, forcing it, so leading to unphysical results; we had never found such a situation in the previous AIMP embedded cluster calculations performed in our group, but we have just met the problem in an attempt to study $CeAlO_3$. For example, we found an occupied $4f$ orbital of a single Ce^{3+} ion embedded in a large ensemble of cubic perovskite $CeAlO_3$ unit cells with origin in Ce sites, to have a positive orbital energy of 0.3206 hartree, which is rised 0.43524 hartree when the unit cell origin is chosen to be the Al site. This is so because the electrostatic potential at the Ce site created by an infinite array of $CeAlO_3$ unit cells with cubic perovskite structure is -0.81088 hartree if the unit cells have their origin at Ce and -1.24612 hartree if they have their origin at Al. Obviously, the same shift is experienced by the whole electrostatic potential map: for instance, its value in the O site is 1.04530 hartree in the first case and

0.61006 hartree in the second case, the potential difference between O and Ce sites being 1.85618 hartree in both cases, which illustrates the arbitrariness mentioned above.

Having recognized the implicit arbitrariness involved in the traditional choice $B_k = -2\,\varepsilon_k$, which was effective so far, we propose in this paper a new procedure to determine B_k values of embedding AIMPs. The underlying idea is to keep the basic philosophy of the AIMPs, namely, that each term of an AIMP is chosen so that it mimics the effects of the true operator it represents, although at a lower computational cost.[10] Since (a) the B_k's represent the strength of the Pauli repulsion and (b) inadequate treatments of Pauli repulsion in embedded cluster calculations lead to inaccurate cluster structures as the main direct effect,[18] the B_k's of a host are chosen in the new procedure so that small embedded clusters of the host have the same local structures as much larger, reference embedded clusters. In this way, we expect that the Pauli repulsion between the small cluster and its environment as taken into account by the AIMP term, mimics the Pauli repulsion between the inner and outer regions of the large cluster. For this to be so, it is neccessary, first, that the remaining terms of the embedding AIMP (Coulomb and exchange) properly mimic their corresponding interactions, something which is intrinsic to the AIMP method,[1] and, second, that the levels of the calculations on the small and the large clusters are equivalent. In order to fulfil the latter condition, having in mind that AIMP embedded clusters are approximations to frozen-environment embedded clusters, the reference calculations on large clusters are made using flexible basis sets in the innermost region that corresponds to the small cluster and minimal basis sets for the outermost regions, which are represented by embedding AIMPs in the small embedded cluster calculation.

The B_k-dependent terms and the entire embedding potentials so produced are expected to represent the Pauli repulsion and the embedding interactions within the host adequately and, by extension, to perform equally well in embedded cluster calculations when impurities and other kind of local defects are introduced in the host.

The new procedure to obtain corrected embedding AIMPs is described in detail in Sec. II. Embedding AIMPs for $CeAlO_3$, CeO_2, and UO_2 have been computed following the new procedure and they are presented in Sec. III.

II. METHOD

A. Embedding AIMPs

The starting point of the embedding AIMPs is the application of the group function theory to two groups of electrons without mutual correlation[6–8] (the cluster and the host electrons in this case), according to which the many electron wave functions of the cluster under the effects of the embedding host can be computed out of the following embedded cluster Hamiltonian,

$$\hat{H}_{\substack{\text{embedded}\\\text{cluster}}} = \hat{H}_{\substack{\text{isolated}\\\text{cluster}}} + \sum_{i}^{\substack{\text{cluster}\\\text{electrons}}} \left\{ -\sum_{\xi}^{\substack{\text{host}\\\text{nuclei}}} \frac{Z_\xi}{r_{\xi i}} + \sum_{\mu}^{\substack{\text{host}\\\text{orbitals}}} \left[f_\mu \int \frac{\varphi_\mu^*(j)[2-\hat{P}_{ij}]\varphi_\mu(j)}{r_{ij}} d\tau_j + B_\mu |\varphi_\mu\rangle\langle\varphi_\mu| \right] \right\} \quad (1)$$

The last terms in Eq. 1 represent the following interactions of the cluster electrons: firstly, the electrostatic interaction with the host nuclei; secondly, the Coulomb and exchange interactions with the host electrons, whose charge density is represented by means of the occupied orbitals φ_μ (with fractional occupancies f_μ); and thirdly, the Pauli repulsion with the latter (last term with positive values of B_μ), which is positive for non-converged cluster orbitals and prevents the collapse of these onto the host orbitals, and so their over occupancy, and is zero for fully converged cluster orbitals in the basis set limit. This embedded cluster Hamiltonian can be used at any level of theory within the cluster. It mantains the cluster electron count since no charge transfer is formally allowed between the cluster orbitals and the environment orbitals.

The φ_μ set in Eq. 1 can be any unitary transformation of the occupied host orbitals, so that both delocalized and localized orbitals can be used. In an ionic crystal, host localized orbitals can often be found that only contain small mixing between orbitals of the individual ions, ϕ_k^ξ; in these cases, substituting the φ_μ set by the ϕ_k^ξ set can be a reasonable approximation. The AIMP embedded cluster Hamiltonian results from adopting such an approximation and substituting the Coulomb and exchange operators by model potential representations of them,[1,2]

$$\hat{H}_{\substack{\text{embedded}\\\text{cluster}}} = \hat{H}_{\substack{\text{isolated}\\\text{cluster}}} + \sum_{i}^{\substack{\text{cluster}\\\text{electrons}}} \sum_{\xi}^{\substack{\text{host}\\\text{ions}}} \hat{V}_\xi^{\text{AIMP}}(i)\,, \quad (2)$$

where the embedding AIMP of the host ion ξ reads

$$\hat{V}_{\xi}^{\mathrm{AIMP}}(i) = -\frac{Q_{\xi}}{r_{\xi i}} + \frac{1}{r_{\xi i}} \sum_{p} C_{p}^{\xi} \exp(-\alpha_{p}^{\xi} r_{\xi i}^{2}) + \sum_{p} \sum_{q} |\chi_{p}^{\xi}\rangle A_{pq}^{\xi} \langle \chi_{q}^{\xi}| + \sum_{k} B_{k}^{\xi} |\phi_{k}^{\xi}\rangle \langle \phi_{k}^{\xi}| \,, \tag{3}$$

with:

$$Q_{\xi} = Z_{\xi} - N_{\xi}^{\mathrm{elec}} \,, \tag{4}$$

so that the first term is the ionic point charge potential;

$$\frac{1}{r_{\xi i}} \sum_{p} C_{p}^{\xi} \exp(-\alpha_{p}^{\xi} r_{\xi i}^{2}) \approx -\frac{N_{\xi}^{\mathrm{elec}}}{r_{\xi i}} + 2 \sum_{k} f_{k} \int \frac{\phi_{k}^{\xi *}(j) \phi_{k}^{\xi}(j)}{r_{ij}} d\tau_{j} \,, \tag{5}$$

with the sets C_{p}^{ξ} and α_{p}^{ξ} chosen to minimize the deviations, so that the second term corrects the point charge potential with the electrostatic contributions from the ionic electron density; and

$$A_{pq}^{\xi} = -\sum_{r} \sum_{s} S_{pr}^{-1} \sum_{k} f_{k} \int \frac{\chi_{r}^{\xi *}(i) \phi_{k}^{\xi *}(j) \phi_{k}^{\xi}(i) \chi_{s}^{\xi}(j)}{r_{ij}} d\tau_{j} d\tau_{i} S_{sq}^{-1} \,, \tag{6}$$

with the S matrix defined by

$$S_{pq} = \langle \chi_{p}^{\xi} | \chi_{q}^{\xi} \rangle \,, \tag{7}$$

so that the third term is the exchange interaction between the embedding electrons and the i-th cluster electron, in the form of a spectral representation (resolution of the identity). In Eqs. 3, 6 and 7, the χ_{p}^{ξ} are a set of auxiliar functions; usually, these are the primitive Gaussians used to expand the ion orbitals ϕ_{k}^{ξ}. The B_{k}^{ξ} set in the last term are positive constants, whose calculation is the subject of this paper.

B. Self-consistent embedded ions

The first step in the calculation of the components of the embedding AIMP of an ionic solid made of monoatomic ions, like CeO_2, is the self-consistent embedded ions procedure, SCEI. (An extension of the embedding AIMP method for multiatomic ions has been recently implemented,[19] but it will not be used in this work.) It starts with the assumption of an ionic limit for the host and with the identification of its ions; in the sample case these are Ce^{4+} and O^{2-}. For each of these ions, a first calculation (e.g. Hartree-Fock) is performed on the ground

state of the ion embedded in an initial environmental potential (e.g. that corresponding to a point charge representation of all the other crystal ions) and its embedding AIMP is produced out of its occupied orbitals according to Sec. II A. At this step, $B_k = -2\,\varepsilon_k$ is used for the orbitals in fully occupied shells, except when positive orbital energies are found, in which case a fixed value is adopted, usually $B_k = 0.5$ au. Other positive B_k values large enough so as to prevent orbital collapses onto the external lattice (which should always be monitored) are equally valid here because they will be changed in a forthcoming tunning step. $B_k = 0$ is used for the orbitals in partially occupied shells, because these shells should not be prevented from additional occupancy. The new embedding AIMP is used to update the environmental potentials of all ions. Then, a new set of calculations on the individual embedded ions is carried out, new embedding AIMPs are produced, and so on. The iterations are stopped when the wave functions, total energies and orbital energies of the embedded ions have converged. At this point, all the ingredients of the embedding AIMPs of the individual ions (Eq. 3) are stored in libraries, although the B_k^ξ constants will be modified as described next.

C. Frozen-orbital shifting operator

The B_k constants in the frozen-orbital shifting operator of the embedding AIMPs,

$$\sum_{\xi}^{\substack{\text{host}\\ \text{ions}}} \sum_{k}^{\substack{\text{orbitals}\\ \text{of } \xi}} B_k^\xi |\phi_k^\xi\rangle\langle\phi_k^\xi| \,, \tag{8}$$

will be tuned in embedded cluster calculations. In order to lead the tuning procedure, we recall that the true embedding potential that the embedding AIMP intends to mimic corresponds to an environment whose electrons occupy frozen orbitals which have been calculated at the SCF level.[1,7] Then, the best result we can expect out of an AIMP embedded cluster calculation on a system, at a given methodological level for the cluster, is one that coincides with another calculation on the whole system, where the cluster is treated at the same methodological level whereas the rest of the system is treated at a SCF level, with its orbitals frozen to the result of the SCF calculation on the whole system.

With this idea in mind, for a given host (e.g. CeO_2), we perform SCF calculations on one or several small working clusters (e.g. $(CeO_8)^{12-}$, if we are interested in local properties of CeO_2 associated with one cation or with impurities and other defects related with it) and on

corresponding large reference clusters (e.g. $(CeO_8Ce_{12}O_{56})^{76-}$). For simplicity, we will refer to the above clusters and alike as *small* and *reference* clusters from now on. Both types of clusters are embedded in the embedding AIMP resulting from the previous SCEI calculation (Sec. II B). The SCF calculations are closed-shell Hartree-Fock calculations in closed-shell clusters and CASSCF calculations in open-shell clusters. A large, flexible basis set is used for the small cluster as well as for the corresponding, inner region of the reference cluster (i.e. the CeO_8 part). A minimal basis set is used for the outer region of the reference cluster, which corresponds to an embedding part in the small cluster calculation (i.e. the $Ce_{12}O_{56}$ part). The minimal basis set functions are the orbitals (of Ce^{4+} and O^{2-}) resulting from the previous SCEI calculation. It is reasonable to think that, under these conditions, the Coulomb and exchange terms of the embedding AIMP used in the small cluster calculation represent fairly well the Coulomb and exchange interactions between the outer and the inner regions in the reference cluster calculation. On the other hand, the choice of B_k's made in the SCEI calculation does not neccessarily make the frozen-orbital shifting operator (Eq. 8) to represent correctly the Pauli repulsion interactions between the small cluster and its environment, as discussed above. Then, since inaccurate Pauli repulsions produce inaccurate geometrical parameters,[18] it is reasonable to think that the differences between the small cluster structures, as computed in the small cluster and in the reference cluster calculations, are mostly ascribable to the frozen-orbital shifting operator not properly mimiking the Pauli repulsion interactions between the inner and outer regions of the reference cluster. A simple way to correct this is tuning the B_k constants so that the SCF calculations on the small clusters embedded in B_k-corrected embedding AIMPs give the same local structure than the SCF calculations on the reference clusters, and this is what we do here.

In practice, several sets of B_k constants are able to fulfil the structural criterion just described. In order to make a final choice, we use the additional demand that none of the constants should be small, meaning that, among one set with large and small constants and another with evenly distributed medium size constants, we chose the latter. Finally, we find convenient to check that the chosen B_k constants are such that states with occupied orbitals of a more diffuse character than those of the ground state do not collapse on the external lattice either. Examples are: states of the $5d^1$ configuration of Ce^{3+} in $CeAlO_3$, $4f^1$ and $5d^1$ states of a Ce^{3+} dopant in CeO_2, or states of the $5f^16d^1$ configuration of U^{4+} in UO_2.

We expect the embedding potentials so obtained to perform equally well than alternative

potentials with B_k constants tuned in more expensive, correlated small and reference embedded cluster calculations, as long as the correlation in the reference cluster is restricted to the inner region, because the AIMPs are designed to mimic the effects of the frozen embedding region and this would be the same in the SCF and in the correlated calculations. This will be illustrated later with SCF and second-order perturbation theory calculations.

D. Embedding self-consistency

After the first SCEI calculation (Sec. II B) and B_k tuning (Sec. II C), the embedding orbitals ϕ_k^ξ and shifting constants B_k^ξ are not fully consistent. In order to make them so, iterative cycles are started consisting of a new SCEI calculation using the last tuned constants, followed by a new B_k tuning. The cycles are stopped when the orbitals and constants do not change significantly.

III. RESULTS

We obtained the embedding AIMPs of $CeAlO_3$, CeO_2, and UO_2, following the method described in Sec. II. All the calculations were performed with MOLCAS.[20]

For $CeAlO_3$, we adopted the high temperature cubic perovskite structure,[21] corresponding to the $Pm\overline{3}m$ spatial group, with lattice constant a_0=3.818 Å. In this host, Ce(III) and Al(III) are 12-fold and 6-fold coordinated with oxygens, respectively. We took the Ce-O and Al-O distances as the target structural parameters, so that the small and the reference embedded cluster calculations should lead to the same values of them. We chose $(CeO_{12})^{21-}$ and $(AlO_6)^{9-}$ as small clusters, and $(CeO_{12}Al_8Ce_{26}O_{24})^{33+}$ and $(AlO_6Al_{26}Ce_8O_{48})^{3-}$ as the corresponding reference clusters (see Fig. 1). All of them were embedded in an AIMP representation of $CeAlO_3$ where all the ions external to the clusters are located at experimental sites (ions up to 2 unit cells far from the central cation are represented by total-ion AIMPs and the remaining ions up to 6 unit cells away are represented by point charges, using Evjen's fractional values for the ions on the edges of the embedding region for a faster convergence of the electrostatic potential[22]).

The SCF calculations involved in the SCEI calculations were defined as follows: For Ce^{3+}, complete active space SCF calculations, CASSCF,[23–25] were done on the lowest Stark com-

ponent of $4f^1\ ^2F$, using a relativistic [Kr] core AIMP and a $(14s10p10d8f)/[7s5p6d4f]$ Gaussian basis set[26,27]; for Al^{3+} and O^{2-}, all-electron closed-shell Hartree-Fock calculations were performed with uncontracted $(11s8p)$ and $(8s6p)$ Gaussian basis sets,[28] respectively. The SCF calculations on the small and the reference embedded clusters were done at the Hartree-Fock level on the Al-centered clusters and at the CASSCF level (on the $4f(a_{2u})^1\ ^2A_{2u}$ state) on the Ce-centered clusters. In $(AlO_6)^{9-}$, an all-electron ANO-S $[5s4p2d]$ basis set was used for Al[29] and a [He] core AIMP with a $(5s6p1d)/[2s3p1d]$ basis for O.[13] In $(CeO_{12})^{21-}$, the Ce basis set was the same as in the SCEI calculation, augmented with g polarization functions, $(14s10p10d8f3g)/[7s5p6d4f1g]$, and the O basis set was the same as in $(AlO_6)^{9-}$. In both small clusters, the basis sets were extended with additional functions located on first shell neighbors: in $(AlO_6)^{9-}$, on the six Al atoms next to O along the Al-O axes; in $(CeO_{12})^{21-}$, on the twelve Ce atoms next to O along the Ce-O axes and on the eight Al atoms closest to Ce (see Fig. 1). The additional functions are a $[1s1p1d]$ set for Ce and a $[1s1p]$ set for Al, made with the $4d$, $5s$, and $5p$ orbitals of Ce^{3+} and the $2s$ and $2p$ of Al^{3+}, respectively, as obtained in the previous SCEI calculations. The basis sets used for the large, reference clusters were the same as in the small clusters for the common atoms, AlO_6 and CeO_{12} respectively, and the following minimal basis sets for the remaining atoms, $Ce_8Al_{26}O_{48}$ and $Ce_{26}Al_8O_{24}$, respectively: [He] core AIMP plus $(8s6p)/[1s1p]$ for O, [He] core AIMP plus $(11s8p)/[1s1p]$ for Al, and [Kr,4f] core AIMP plus $(14s10p10d)/[1s1p1d]$ for Ce; in all of them, the orbitals used in the frozen-core AIMP and in the minimal basis sets were the atomic orbitals resulting from the previous SCEI calculation on the host.

The summary of the calculation of the frozen-orbital shifting constants B_k of $CeAlO_3$ is presented in Table I. The full embedding AIMPs of this and the other hosts of this paper can be obtained from the authors upon request or on-line.[30] The B_k's of the SCEI calculation produce a less repulsive barrier than the correct Pauli repulsion and, as a result, the bond lenthgs obtained in the small cluster calculations before the B_k tuning are too long. Increasing the shifting constants of some of the outer orbitals in the B_k tuning step is sufficient to correct for this behaviour. After two cycles, the orbitals and the shifting constants used in the embedding potential are consistent. The SCF distances calculated in the reference and in the small clusters agree with the experimental ones within 0.01 Å. Inclusion of dynamic correlation via second-order perturbation theory corrections (correlating all the valence electrons of the small clusters) shortens both distances, as expected, and slightly

increases the deviations with experiment to around 0.02-0.03 Å, or 1%, which is normal for the system and level of calculation. It is interesting to observe that, although the improved embedding potential has been calculated using a criterion of consistency of ground state SCF geometries of small and large clusters, the consistency is mantained at the correlated level, PT2. In order to check that the consistency extends to excited states of the same and of different configurations, we present in Table II the results of the bond lengths of the $^2T_{1u}$, $^2T_{2u}$, and ^2A_u states of the $4f^1$ configuration of Ce^{3+} centered clusters, as well as on the ^2E_g and $^2T_{2g}$ states of the $5d^1$ configuration. As it can be seen, geometries and transition energies computed with the large and the small embedded clusters largely agree.

CeO_2 has the fluorite structure ($O_h^5 - Fm3m$, $a_0 = 5.411$ Å).[31] In it, Ce(IV) is 8-fold coordinated with oxygens and we took the Ce-O distance as the target structural parameter. We chose $(CeO_8)^{12-}$ and $(CeO_8Ce_{12}O_{56})^{76-}$ as the small and corresponding reference clusters, respectively (see Fig. 2). We embedded both of them in an AIMP representation of the CeO_2 lattice where all the ions external to the cluster are located at experimental sites, with a number of total-ion AIMPs and point charges equivalent to $CeAlO_3$. In the SCEI procedure, we performed SCF calculations on the Ce^{4+} and O^{2-} ions using the same AIMPs and basis sets described for the SCEI calculations on $CeAlO_3$. For the SCF calculations on the small embedded cluster $(CeO_8)^{12-}$, we used the same AIMPs and basis sets described for the $(CeO_{12})^{21-}$ cluster of $CeAlO_3$, extended with additional functions located on the first shell of neighbor Ce sites, which have been the $4d$, $5s$, and $5p$ orbitals of Ce^{4+} obtained in the previous SCEI calculation on the CeO_2 host, totally contracted as $[1s1p1d]$. For the SCF calculations on the reference embedded cluster $(CeO_8Ce_{12}O_{56})^{76-}$, we used the same basis sets as in $(CeO_8)^{12-}$ for the innermost Ce and O atoms, and the following minimal basis set for the remaining $Ce_{12}O_{56}$ atoms: [He] core AIMP plus $(8s6p)/[1s1p]$ for O and [Kr] core AIMP plus $(14s10p10d)/[1s1p1d]$ for Ce.

The summary of the calculation of B_k parameters of CeO_2 is shown in Table III. The results are in line with those previously described for $CeAlO_3$ and an increasing of the B_{5p}^{Ce} constant in the tuning step together with a small reduction of B_{2p}^{O} is enough to correct the originally insufficiently repulsive barrier in the small cluster. After three cycles we find consistency between the orbitals and the shifting parameters. It can be noticed that the deviations with experiment of the calculated structural parameters is around 0.04 Å, somewhat larger than that found in $CeAlO_3$. Dynamic correlation effects, as included by means

of MBPT2 calculations (correlating all the valence electrons of the clusters), additionaly shorten 0.02 Å the Ce-O distances of the small and reference clusters, with a final deviation with experiment of approximately 3 %. Monitoring calculations on states of a $(CeO_8)^{13-}$ embedded cluster which correspond to $4f^1$ and $5d^1$ configurations of a Ce^{3+} impurity (electron doping of CeO_2) did not reveal any problems of electron leaking off the cluster and collapase onto the external lattice.

UO_2 is isomorphous with CeO_2 and we treated it in a parallel manner. At room temperature, UO_2 exhibits a fluorite structure with lattice constant $a_0 = 5.470$ Å.[32] U(IV) is 8-fold coordinated with oxygens and we took the U-O distance as the target structural parameter. We chose $(UO_8)^{12-}$ and $(UO_8U_{12}O_{56})^{76-}$ as the small and reference clusters, respectively (see Fig. 2), and we embedded both of them in an AIMP representation of the UO_2 lattice similar to that used for CeO_2, with all the ions external to the cluster located at experimental sites. The SCF calculations involved in the SCEI procedure were similar to those proposed for $CeAlO_3$. For the U atoms, a relativistic [Xe,$4f$] core AIMP was used in combination with a $(14s10p12d9f)/[4s3p4d4f]$ basis set.[26,27] To describe the U^{4+} ion, a CASSCF calculation on the lowest Stark component of $5f^2\ ^3H$ was performed. O^{2-} was treated as in $CeAlO_3$. For the small and reference embedded clusters, the calculations were done at the CASSCF level on the ground state (the first $^3T_{1g}$ state of dominant $5f^2$ character, at this level). For the central U atom, a relativistic [Xe,$4f$] core AIMP was used in combination with a $(14s10p12d9f3g)/[6s5p6d4f2g]$ basis set.[26,27] O atoms were treated with a [He] core AIMP plus $(5s6p1d)/[2s3p1d]$. In the small cluster $(UO_8)^{12-}$, the basis sets were extended with additional functions located on the first shell of neighbor U sites. As previously, these functions were made with the outermost $5d$, $6s$, and $6p$ atomic orbitals obtained in the SCEI calculation of U^{4+} embedded in UO_2, contracted as $[1s1p1d]$. In the large, reference cluster $(UO_8U_{12}O_{56})^{76-}$, the 12 peripheral U atoms were described with a [Xe,$4f^{14}$,$5f^2$] core AIMP made out of the SCEI orbitals of U^{4+}, in combination with a $(14s10p12d)/[1s1p1d]$ minimal basis set to describe the $6s$, $6p$, and $5d$ orbitals. Likewise, the 56 peripheral O atoms were described with a [He] core AIMP and a $(8s6p)/[1s1p]$ minimal basis set from the SCEI calculation of O^{2-} embedded in UO_2.

The B_k parameters of UO_2 are shown in Table IV. As previously, with the initial B_k values, the optimized U-O distance is longer for the small cluster (2.430 Å) than for the reference cluster (2.338 Å). To correct this discrepancy, the B_k values corresponding to the

outermost orbitals ($5d$, $6s$, $6p$ of U, and $2s$, $2p$ of O) were uniformly risen. Consistency between the orbitals and the shifting parameter is achieved after two cycles. The final U-O distance is 0.03 Å shorter than the experimental distance. Dynamic correlation effects included at the CASPT2 shortens the distance to 2.315 Å. The final deviation with experiment is 0.055 Å, approximately 2%. States of the $(UO_8)^{12-}$ embedded cluster corresponding to the excited $5f^16d^1$ configuration of U^{4+} are calculated without further difficulties with the present embedding potential. A detailed study of the complex $5f^2$ and $5f^16d^1$ manifolds of UO_2 will be presented elsewhere.[33]

IV. CONCLUSIONS

In this paper, we propose a method to produce improved embedding *ab initio* model potentials for embedded cluster calculations in ionic solids and we apply it to three oxides, namely, the cubic perovskite $CeAlO_3$ and the CeO_2 and UO_2 hosts with fluorite structure. The improvement with respect to the former version of the embedding AIMP method[1] consists of a new calculation of the embedding term that represents the Pauli repulsions between the embedded cluster and its environment, under a criterion of consistency of ground state structures with respect to the size of the embedded clusters.

Acknowledgments

This work was partly supported by a grant from Ministerio de Ciencia e Innovación, Spain (Dirección General de Programas y Transferencia de Conocimiento MAT2008-05379/MAT).

---

* Corresponding author; Electronic address: `luis.seijo@uam.es`

[1] Z. Barandiarán and L. Seijo, J. Chem. Phys. **89**, 5739 (1988).

[2] L. Seijo and Z. Barandiarán, in *Computational Chemistry: Reviews of Current Trends*, edited by J. Leszczyński (World Scientific, Singapore, 1999), vol. 4, pp. 55–152.

[3] L. Seijo and Z. Barandiarán, in *Relativistic Electronic Structure Theory: Part 2. Applications*, edited by P. Schwerdtfeger (Elsevier, Amsterdam, 2004), pp. 417–475.

[4] F. Ruipérez, Z. Barandiarán, and L. Seijo, J. Chem. Phys. **127**, 144712 (2007).

[5] J. Gracia, L. Seijo, Z. Barandiarán, D. Curulla, H. Niemansverdriet, and W. van Gennip, J. Lumin. **128**, 1248 (2008).

[6] R. McWeeny, Rev. Mod. Phys. **32**, 335 (1960).

[7] S. Huzinaga and A. A. Cantu, J. Chem. Phys. **55**, 5543 (1971).

[8] S. Huzinaga, D. McWilliams, and A. A. Cantu, Adv. Quantum Chem. **7**, 187 (1973).

[9] Y. Sakai, E. Miyoshi, M. Klobukowski, and S. Huzinaga, J. Comput. Chem. **8**, 226 (1987).

[10] S. Huzinaga, L. Seijo, Z. Barandiarán, and M. Klobukowski, J. Chem. Phys. **86**, 2132 (1987).

[11] S. Huzinaga, J. Mol. Struct.: THEOCHEM **80**, 51 (1991).

[12] G. Höjer and J. Chung, Int. J. Quantum Chem. **14**, 623 (1978).

[13] Z. Barandiarán and L. Seijo, Can. J. Chem. **70**, 409 (1992).

[14] Y. Osanai, M. S. Mon, T. Noro, H. Mori, H. Nakashima, M. Klobukowski, and E. Miyoshi, Chem. Phys. Lett. **452**, 210 (2008).

[15] L. Seijo and Z. Barandiarán, J. Math. Chem. **10**, 41 (1992).

[16] L. G. M. Pettersson and U. Wahlgren, Chem. Phys. **69**, 185 (1982).

[17] L. N. Kantorovich and I. I. Tupitsyn, J. Phys.: Condens. Matter **11**, 6159 (1999).

[18] J. L. Pascual, J. Schamps, Z. Barandiarán, and L. Seijo, Phys. Rev. B **74**, 104105 (2006).

[19] B. Swerts, L. F. Chibotaru, R. Lindh, L. Seijo, Z. Barandiarán, S. Clima, K. Pierloot, and M. F. A. Hendrickx, J. Chem. Theory Comput. **4**, 586 (2008).

[20] G. Karlström, R. Lindh, P. A. Malmqvist, B. O. Roos, U. Ryde, V. Veryazov, P. O. Widmark, M. Cossi, B. Schimmelpfennig, P. Neogrady, and L. Seijo, Comput. Mater. Sci. **28**, 22 (2003).

[21] W. T. Fu and D. J. W. Ijdo, J. Solid State Chem. **179**, 2732 (2006).

[22] H. M. Evjen, Phys. Rev. **39**, 675 (1932).

[23] B. O. Roos, P. R. Taylor, and P. E. M. Siegbahn, Chem. Phys. **48**, 157 (1980).

[24] P. E. M. Siegbahn, A. Heiberg, B. O. Roos, and B. Levy, Phys. Scr. **21**, 323 (1980).

[25] P. E. M. Siegbahn, A. Heiberg, J. Almlöf, and B. O. Roos, J. Chem. Phys. **74**, 2384 (1981).

[26] L. Seijo, Z. Barandiarán, and E. Harguindey, J. Chem. Phys. **114**, 118 (2001).

[27] L. Seijo, Z. Barandiarán, and B. Ordejón, Mol. Phys. **101**, 73 (2003).

[28] J. Andzelm, M. Klobukowski, E. Radzio-Andzelm, Y. Sakai, and H. Tatewaki, *Gaussian Basis Sets for Molecular Calculations*, edited by S. Huzinaga, (Elsevier, Amsterdam, 1984).

[29] K. Pierloot, B. Dumez, P.-O. Widmark, and B. O. Roos, Theor. Chim. Acta **90**, 87 (1995).

[30] Detailed core and embedding AIMP data libraries in electronic format are available from

the authors upon request or directly at the address http://www.uam.es/quimica/aimp/Data/-AIMPLibs.html. See also Ref. 20.

[31] R. W. G. Wyckoff, *Crystal Structures* (Wiley, New York, 1963).

[32] G. Amoretti, A. Blaise, R. Caciuffo, J. M. Fournier, M. T. Hutchings, R. Osborn, and A. D. Taylor, Phys. Rev. B **40**, 1856 (1989).

[33] N. Barros, L. Seijo, and Z. Barandiarán, in preparation.

TABLE I: Frozen-orbital shifting operator constants (B_k, Eq. 8, in hartree) of the AIMP embedding potential of $CeAlO_3$, as obtained from ground state embedded cluster SCF calculations. Distances corresponding to second order perturbation theory, PT2, using the corrected AIMP embedding potential, are shown in parentheses.

			B_k constants[a]		Structural parameters[b]	
Cycle	Clusters	Embedding	B_{5p}^{Ce}	B_{2p}^{O}	d(Ce-O)/Å	d(Al-O)/Å
1	Reference[c]	Initial SCEI	1.372	0.1926	2.689	1.907
	Small[d]	Initial SCEI	1.372	0.1926	2.840	1.998
	Small[d]	B_k tuning	4.000	1.025	2.692	1.905
2	Reference[c]	SCEI after cycle 1	4.000	1.025	2.687	1.900
	Small[d]	SCEI after cycle 1	4.000	1.025	2.702	1.912
	Small[d]	B_k tuning	4.000	1.165	2.688	1.900
3	Reference[c]	SCEI after cycle 2	4.000	1.165	2.689 (2.673)	1.903 (1.896)
	Small[d]	SCEI after cycle 2	4.000	1.165	2.689 (2.673)	1.901 (1.894)

[a]Fixed B_k constants are: $B_{4f}^{Ce} = 0$, $B_{5s}^{Ce} = 2.995$, $B_{2s}^{Al} = 9.0743$, $B_{2p}^{Al} = 5.7093$, and $B_{2s}^{O} = 1.6251$.

[b]Experimental data from Ref. 21 are d(Ce-O)=2.700 Å and d(Al-O)=1.909 Å.

[c]The reference embedded clusters are $(CeO_{12}Al_8Ce_{26}O_{24})^{33+}$ and $(AlO_6Al_{26}Ce_8O_{48})^{3-}$.

[d]The small embedded clusters are $(CeO_{12})^{21-}$ and $(AlO_6)^{9-}$.

TABLE II: Calculated $4f^1$ and $5d^1$ Ce-O bond lengths, R_e (in Å), and $4f \rightarrow 4f$ and $4f \rightarrow 5d$ adiabatic transition energies, T_e (in cm^{-1}), of $CeAlO_3$, using the reference cluster and the small cluster, both of them embedded in the corrected AIMP embedding potential.

	Ref. cluster $(CeO_{12}Al_8Ce_{26}O_{24})^{33+}$				Small cluster $(CeO_{12})^{21-}$			
	SCF		PT2		SCF		PT2	
State	R_e	T_e	R_e	T_e	R_e	T_e	R_e	T_e
$4f^1-{}^2T_{1u}$	2.688	0	2.673	0	2.688	0	2.673	0
$4f^1-{}^2A_{2u}$	2.688	460	2.673	200	2.688	500	2.673	240
$4f^1-{}^2T_{2u}$	2.690	1470	2.673	1280	2.690	1520	2.674	1330
$5d^1-{}^2E_g$	2.690	37680	2.676	35740	2.690	37400	2.674	34980
$5d^1-{}^2T_{2g}$	2.694	44840	2.680	43610	2.695	44930	2.680	43070

TABLE III: Frozen-orbital shifting operator constants, B_k (in hartree), of the AIMP embedding potential of CeO_2, as obtained from ground state embedded cluster SCF calculations.

Cycle	Cluster	Embedding	B_k constants[a] B^{Ce}_{5p}	B^{O}_{2p}	Structural parameter[b] d(Ce-O)/Å
1	Reference[c]	Initial SCEI	0.4627	1.8376	2.306
	Small[d]	Initial SCEI	0.4627	1.8376	2.419
	Small[d]	B_k tuning	1.5000	1.4500	2.306
2	Reference[c]	SCEI after cycle 1	1.5000	1.4500	2.304
	Small[d]	SCEI after cycle 1	1.5000	1.4500	2.308
	Small[d]	B_k tuning	1.5000	1.5200	2.304
3	Reference[c]	SCEI after cycle 2	1.5000	1.5200	2.304
	Small[d]	SCEI after cycle 2	1.5000	1.5200	2.304

[a]Fixed B_k constants are: $B^{Ce}_{5s} = 2.2232$, $B^{O}_{2s} = 3.2772$, and all $Be^{Ce}_{[Kr,4d]}$ and B^{O}_{1s}, which keep their frozen-core values of Refs. 27 and 13.

[b]Experimental value from Ref. 31 is d(Ce-O)=2.343 Å.

[c]The reference embedded cluster is $(CeO_8Ce_{12}O_{56})^{76-}$.

[d]The small embedded cluster is $(CeO_8)^{12-}$.

TABLE IV: Frozen-orbital shifting operator constants, B_k (in hartree), of the AIMP embedding potential of UO_2, as obtained from ground state embedded cluster CASSCF calculations.

Cycle	Cluster	Embedding	B_k constants[a] B^U_{5d}	B^U_{6s}	B^U_{6p}	B^O_{2s}	B^O_{2p}	Structural parameter[b] d(U-O)/Å
1	Reference[c]	Initial SCEI	7.13	2.91	0.70	0.85	0.50	2.338
	Small[d]	Initial SCEI	7.13	2.91	0.70	0.85	0.50	2.430
	Small[d]	B_k tuning	7.95	3.73	1.52	1.67	1.32	2.338
2	Reference[c]	SCEI after cycle 1	7.95	3.73	1.52	1.67	1.32	2.338
	Small[d]	SCEI after cycle 1	7.95	3.73	1.52	1.67	1.32	2.350
	Small[d]	B_k tuning	8.04	3.82	1.61	1.76	1.41	2.339
3	Reference[c]	SCEI after cycle 2	8.04	3.82	1.61	1.76	1.41	2.339
	Small[d]	SCEI after cycle 2	8.04	3.82	1.61	1.76	1.41	2.339

[a]Fixed B_k constants are: $B^U_{5f} = 0$ and all $B^U_{[Xe,4f]}$ and B^O_{1s}, which keep their frozen-core values of Refs. 27 and 13.

[b]Experimental value from Ref. 32 is d(U-O)=2.369 Å.

[c]The reference embedded cluster is $(UO_8U_{12}O_{56})^{76-}$.

[d]The small embedded cluster is $(UO_8)^{12-}$.

Figure captions

FIG. 1: Ce (blue), Al (green), and O (red) atoms of the $(CeO_{12}Al_8Ce_{26}O_{24})^{33+}$ (above) and $(AlO_6Al_{26}Ce_8O_{48})^{3-}$ (below) reference clusters used in $CeAlO_3$. The respective small clusters $(CeO_{12})^{21-}$ and $(AlO_6)^{9-}$ are indicated with larger size atoms and polihedra. Lines indicating the central Ce-O and Al-O axes are also plotted.

FIG. 2: Ce or U (blue) and O (red) atoms of the $(CeO_8Ce_{12}O_{56})^{76-}$ and $(UO_8U_{12}O_{56})^{76-}$ reference cluster used in CeO_2 and UO_2. The respective small clusters $(CeO_8)^{12-}$ or $(UO_8)^{12-}$ are indicated with larger size atoms and polihedra. Lines indicating the central Ce-O or U-O axes are also plotted.

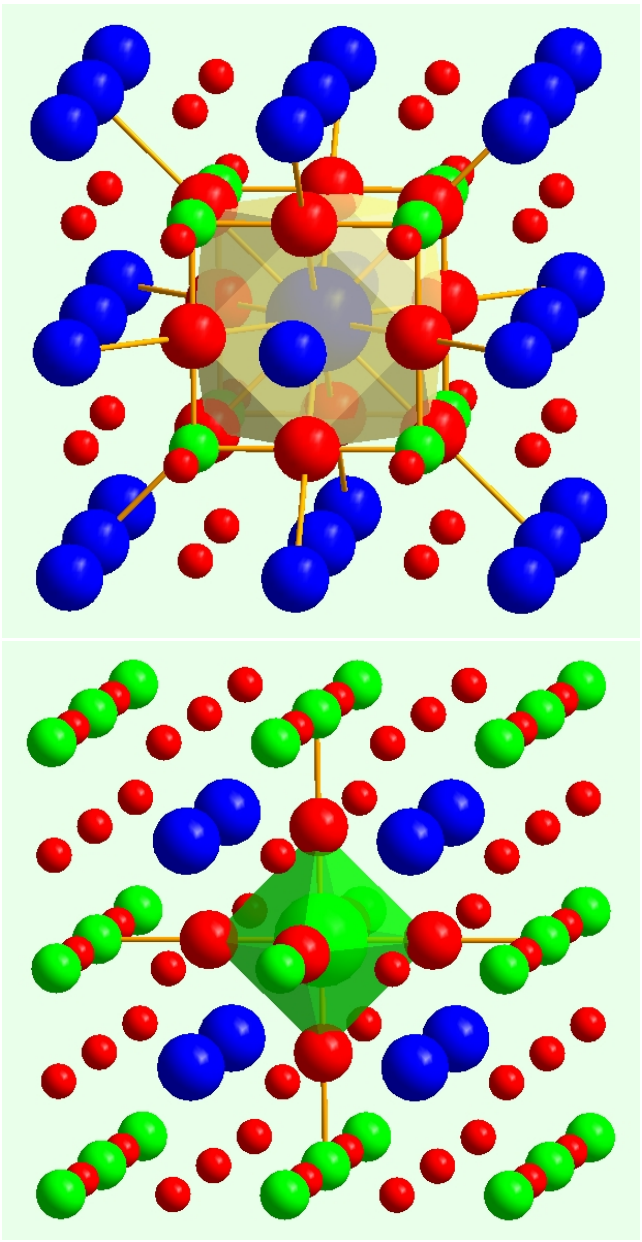

Figure 1. Pascual *et al.*

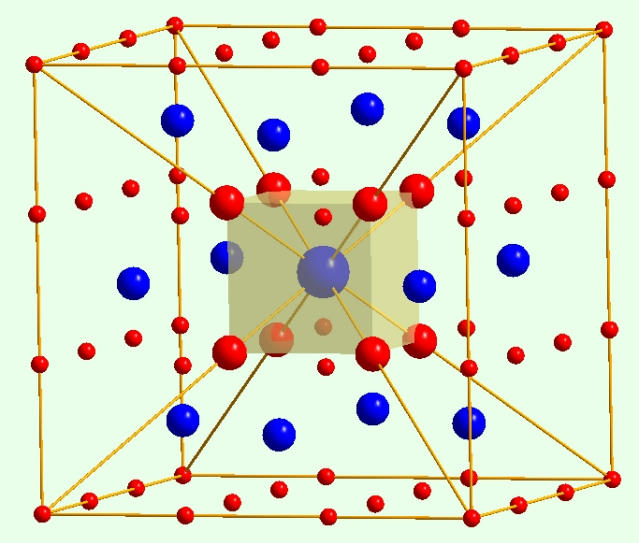

Figure 2. Pascual *et al.*